


Resveratrol Nanoformulation Inhibits Invasive Breast Cancer Cell Growth through Autophagy Induction: An *In Vitro* Study

Mohammad Rasool Khazaei, Ph.D.¹, Maryam Bozorgi, M.Sc.¹, Mozafar Khazaei, Ph.D.¹, Maryam Aftabi, M.D.²,
Azam Bozorgi, Ph.D.^{1,3*} 

1. Fertility and Infertility Research Center, Health Technology Institute, Kermanshah University of Medical Sciences, Kermanshah, Iran
2. Student Research Committee, Kermanshah University of Medical Sciences, Kermanshah, Iran
3. Department of Tissue Engineering, School of Medicine, Kermanshah University of Medical Sciences, Kermanshah, Iran

Abstract

Objective: The aim of this study was to synthesize chitosan nanoparticles (Cs NPs) for resveratrol (RSV) delivery and assess their effectiveness in inducing autophagy in MDA-MB 231 cells.

Materials and Methods: In this experimental study, Pure and RSV-loaded Cs NPs (RSV. Cs NPs) were prepared via the ionic gelation method, and their physicochemical properties were characterized using standard techniques, and RSV release was measured *in vitro*. MDA-MB 231 cells were incubated with RSV, Cs NPs, and RSV. Cs NPs and Half-maximal inhibitory concentration (IC₅₀) values were calculated following the MTT test. Cell viability was assessed by lactate dehydrogenase (LDH) assay, and autophagy was evaluated using the real-time polymerase chain reaction (PCR).

Results: NP formation was confirmed with the analysis of FTIR spectra. Pure and RSV. Cs NPs had 36.7 and 94.07 nm sizes with 18.3 and 27 mV zeta potentials, respectively. Above 60% of RSV entrapped within NPs was released in an initial burst manner followed by a gradual release till 72 hours. Cs and RSV. Cs NPs restrained cell proliferation at lower concentrations. RSV. Cs NPs showed the highest anticancer effect and stimulated autophagy, indicated by increased Beclin-1 ATG5, ATG7, LC3A, and P62 expression.

Conclusion: RSV. Cs NPs show promising effects in inhibiting invasive breast cancer (BC) cells *in vitro* by inducing autophagy.

Keywords: Antineoplastic Effects, Autophagy, Breast Neoplasm, Resveratrol

Citation: Khazaei MR, Bozorgi M, Khazaei M, Aftabi M, Bozorgi A. Resveratrol nanoformulation inhibits invasive breast cancer cell growth through autophagy induction: an *in vitro* study. Cell J. 2024; 26(2): 112-120. doi: 10.22074/CELLJ.2024.2016930.1458

This open-access article has been published under the terms of the Creative Commons Attribution Non-Commercial 3.0 (CC BY-NC 3.0).

Introduction

Breast cancer (BC) is the most diagnosed cancer globally, involving one in eight newly diagnosed cases with a total of 2.3 million, and ranks as the fifth most lethal cancer in both sexes (1). BC is also the most common cancer among females worldwide, with an incidence rate of 25% and a mortality rate of 16%. According to a report by the World Health Organization (WHO), 685000 women died from BC in 2020, and the BC burden is estimated to grow by over 3 million new cases and 1 million deaths in a year By 2040 (2, 3). BC is also among highly prevalent cancers in Iranian women aged 40-50 years, with 16967 newly diagnosed cases in 2020 (1).

Conventional strategies for overwhelming BC involving surgical resection, adjuvant and neo-adjuvant chemotherapy, radiation therapy, and endocrine therapy are restricted by low drug solubility, bioavailability,

poor gastrointestinal permeability, adverse side effects, toxicities, and disease relapse and recurrence (4). Phytochemicals are naturally occurring active compounds from fruits, vegetables, grains, nuts of daily diet, and traditional medicine herbal plants with a long history in cancer research with chemopreventive effects against BC while reducing the dose of administered anticancer drugs and their systemic toxicities (5). Phytochemicals have a variety of pharmaceutical, biological, and health-promoting benefits, such as anti-inflammatory, antioxidant, anticancer, anti-diabetic, cardiovascular, and neuroprotective effects (6, 7).

Resveratrol (RSV, 3, 5, 4'-trans-trihydroxystilbene) is a polyphenolic compound from the stilbene family that abundantly exists in grapes, berries, nuts, and tea (8). Anticancer effects of RSV could be attributed to various mechanisms like inducing apoptosis, cell cycle arrest,

Received: 02/December/2023, Revised: 28/January/2024, Accepted: 05/February/2024

*Corresponding Address: P.O.Box: 6714869914, Fertility and Infertility Research Center, Health Technology Institute, Kermanshah University of Medical Sciences, Kermanshah, Iran
Email: azam.bozorgi@kums.ac.ir



Royan Institute
Cell Journal (Yakhteh)

autophagy, and modulating kinase signaling pathways (9). Despite beneficial pharmaceutical effects, low water solubility, weak bio-availability, and structural instability under physiological conditions entangle the administration of phytochemicals in the native form (10). Over the past few decades, nanotechnological advancements have established nanocarrier systems for the specific delivery of phytochemicals to overcome these challenging issues and enhance their therapeutic efficacy (11).

Nanocarrier-based delivery systems prolong the drug's half-life under the physiological milieu, improve its penetration into the target site, and provide a constant local concentration in situ (12). Nanocarriers augment their cargo's bioavailability and antitumor efficacy while reducing the dose of therapeutics required for the expected effective clinical outcome. Some nanocarrier-based therapeutic strategies are currently being investigated in the clinic for BC treatment (13). Among various nanocarriers used for drug delivery, nanoparticles (NPs) are advantageous for controlling drug distribution and release in the body (14).

Chitosan (Cs) is a deacetylated derivative of chitin, a biopolymer extracted from the crustacean exoskeleton, with unique properties like biodegradability, biocompatibility, safety, non-toxicity, and non-immunogenicity, making it an ideal candidate for NP synthesis and biomedical applications (15). Cs NPs have been widely investigated for the delivery of chemotherapeutic agents like docetaxel (16), doxorubicin (17), and phytochemicals such as curcumin (17) and quercetin (18) for targeted BC therapy. In the present study, we aimed to synthesize RSV. Cs NPs and evaluated their anticancer effect against BC via inducing autophagy.

Materials and Methods

This experimental study was confirmed by the Ethical Committee of the Kermanshah University of Medical Sciences, Kermanshah, Iran (IR.KUMS.MED.REC.1401.250).

Nanoparticle synthesis and characterization

Pure and RSV. Cs NPs were synthesized using a previously described ionic gelation technique with some modifications (19, 20). Cs (Low molecular weight, Cat no. 448869, Sigma, Germany) and Tripolyphosphate (TPP, Cat no. 238503, Sigma, Germany) solutions were prepared in acetic acid (0.5% v/v) and deionized water and ultrasonicated to obtain homogenized solutions. Pure Cs NPs were formed by dropwise mixing 1.25 mg/ml of TPP solution (pH=4) with 2 mg/ml of Cs solution (pH=5) under constant stirring at 700 RPM for 30 minutes (Cs: TPP ratio: 10:1). RSV. Cs NPs were synthesized by adding 3 mg/ml RSV to the Cs solution. NP suspensions were centrifuged at 15000 RPM for 15 minutes at 4°C, pellets were washed in deionized water three times, followed by overnight drying at 40°C (19).

NP formation and their chemical compositions were confirmed by the Fourier transform infrared (FTIR) spectroscopy at 400-4000 cm^{-1} wavelength using the Nexus670 Thermo Nicolet FTIR spectrometer (Gaithersburg, USA). NP suspension was analyzed to determine particle mean size, distribution, and zeta potential using the dynamic light scattering (DLS) method in a Malvern Zetasizer instrument (Malvern Panalytical Ltd, United Kingdom) at room temperature and a scattering angle of 90°. Morphological characteristics of dried NPs were evaluated using the scanning electron microscope (TESCAN ORSAY HOLDING, Brno-Kohoutovice, Czech Republic) following gold coating at 15kV accelerating voltage. The RSV entrapment efficiency (EE) was computed by reading the absorbances of RSV. Cs NP suspension (total RSV) and NP-free supernatants (free RSV) at 310 nm in the Unico 2800 UV/Visible spectrophotometer machine (UNICO, Dayton, NJ, USA). EE was calculated according to the following equation:

$$\text{Entrapment efficiency(\%)} = \frac{\text{Total RSV} - \text{Free RSV}}{\text{Total RSV}} \times 100$$

To evaluate RSV release from NPs, RSV. Cs NPs were suspended in PBS (pH=7.4) and incubated at 37 °C for different time points up to 48 hours. Half of the supernatant was collected and replaced with fresh PBS at each time point. The absorbance of the collected supernatant was read at 310 nm using the Unico 2800 UV/Visible spectrophotometer.

Cell line preparation and culture

The human BC cell line (MDA-MB231, NCBI Code: C578) was purchased from the Pasteur Institute of Iran (Tehran, Iran) and cultured in DMEM-F12 media supplemented with 10% fetal bovine serum (FBS, Gibco Invitrogen, USA), 100 U/ml penicillin, and 100 $\mu\text{g/ml}$ streptomycin and incubated in a humidified chamber under 37 °C and 5% CO_2 pressure conditions. Culture media were changed every three days until cells reached 80% confluency.

Cell proliferation and IC_{50} calculation

an MTT assay (3-(4,5-dimethylthiazol-2-yl)-2,5-diphenyltetrazolium bromide) was performed to evaluate the effect of NPs on MDA-MB 231 cell proliferation (21). MDA-MB 231 cells were cultured in 96-well plates at 10^4 cells/well density. Cells were treated with RSV, Cs NPs, and RSV. Cs NPs (0, 25, 50, 100, 200 $\mu\text{g/ml}$) for 24, 48, and 72 hours. At each time, culture media were discarded, each well was added 200 μL MTT reagent (0.5 mg/ml, in PBS), and the plate was incubated at 37 °C for three hours. After MTT was removed, 200 μL DMSO was added to wells, and optical density (OD) was read at 570 nm using the ELISA reader system (Biorad, Hercules, CA, USA). Cell proliferation was computed according to the equation:

$$\text{Cell (\%)} = (\text{OD}_T) / (\text{OD}_C) \times 100$$

OD_T is the OD of treated cells, and OD_C is the OD of untreated cells.

Half-maximal inhibitory concentration (IC_{50}) values were computed by plotting the dose-response curves in GraphPad Prism 7 software (GraphPad Software, San Diego, CA, USA).

Cell viability

The lactate dehydrogenase (LDH) assay was used to evaluate MDA-MB231 cell viability. LDH is a cytosolic enzyme excreted into the culture media upon cell membrane damage, which could be measured to determine cell damage. After MDA-MB231 cells were cultured at 10^4 cells/well density, they were treated with RSV, Cs NPs, and RSV. Cs NPs (0, 25, 50, 100, and 200 $\mu\text{g/ml}$) for 24, 48, and 72 hours. An additional group of cultured cells was regarded for measuring Total LDH. LDH was assessed by the LDH assay kit (Kiazist, Iran) according to the manufacturer's recommendation. Total LDH was extracted by adding 20 μL Permision solution and incubating the plate for an hour at 25°C . Then, 50 μL supernatant from each well of the Total LDH, control, and treatment groups was collected, mixed with 50 μL working buffer, and incubated at 37°C for 30 minutes. The OD of samples was read at 545 nm using the ELISA reader system, and cell viability was calculated as follows:

$$\text{Cell viability (\%)} = 1 - (\text{OD}_{\text{Test}} - \text{OD}_{\text{Control}}) / (\text{OD}_{\text{Total}} - \text{OD}_{\text{Control}}) \times 100$$

OD_{Test} is the OD of treated cells, and $\text{OD}_{\text{Control}}$ is the OD of untreated cells.

Autophagy measurement

The expression of autophagic genes was assessed using a quantitative two-step Real-time polymerase chain reaction (PCR) technique described elsewhere (19). For this purpose, MDA-MB cells were treated with IC_{50} concentrations of RSV, Cs NPs, and RSV. Cs NPs were incubated under standard culture conditions for 48 hours. Cells that did not receive any treatments were regarded as the control group. After incubation, cell pellets were collected following trypsinization and centrifugation and transferred into Rnase-free microtubes. Total RNAs were extracted using a Trizol agent (Life Biolab, Heidelberg, Germany), and their concentrations were measured using the NanoDrop 2000 Spectrophotometer (Thermo Scientific, Germany, Deutschland). cDNA was synthesized from $1\mu\text{g}$ RNA using the RevertAid First Strand cDNA Synthesis Kit (ThermoFisher Scientific Inc., Porto Salvo, Portugal), as the manufacturer recommended. cDNA was employed for the Real-time polymerase chain reaction (PCR) using the high-ROX SYBR green PCR Master Mix (RealQ Plus 2x Master Mix, Ampliqon, Denmark) in Step One Real-time PCR machine (Applied Biosystems, USA). The obtained comparative threshold cycle (Ct)

was normalized against the glyceraldehyde 3-phosphate dehydrogenase (*GAPDH*), and relative gene expression was calculated as the fold change = $2^{-\Delta\Delta\text{Ct}}$. The forward and reverse primers are listed in the following Table S1 (See Supplementary Online Information at www.celljournal.org).

Statistical analysis

Experiments were performed in triplicates ($n=3$), and quantitative data were reported as Mean \pm S.D. A one-way analysis of variance (ANOVA) followed by Tukey's test was performed in GraphPad Prism 7 software (GraphPad Software, San Diego, CA, USA) at significant levels $P<0.001$ and $P<0.010$.

Results

Nanoparticle synthesis and characterization

In the current experiment, we used a simple ionic gelation technique for synthesizing highly pure and appropriate particle-size blank Cs and RSV. Cs NPs. NP formation was approved visually by appearing as an opaque solution after the dropwise addition of TPP into the Cs solution. The observational data were confirmed by analyzing the chemical structure of NPs using FTIR (Fig.1). Cs FTIR peaks in Cs NPs were detected at 1639 cm^{-1} , 2924 cm^{-1} , and 3437 cm^{-1} , belonging to C=O stretching (amide I), C-H symmetric stretching, and O-H stretching, respectively. TPP peaks in Cs NPs were detected at 1150 cm^{-1} and 1207 cm^{-1} , attributed to P=O bonds and asymmetric stretching of the PO_2 group. Cross-linking between Cs and TPP was observed as a peak at 1572 cm^{-1} , correlated to N-O-P stretching. In the case of RSV. Cs NPs, additional small peaks at 1386.8 cm^{-1} , 1512 cm^{-1} , and 1581 cm^{-1} were attributed to RSV structure, including C=O stretching, benzene ring, and aromatic ring C=C stretching.

The morphological evaluation of NPs with SEM is shown in Figure 2A. Dried NPs were highly agglomerated, while single NPs (yellow arrows) were spherical with smooth surfaces distributed in nanometric dimensions. NP size, distribution, and surface charges measured by DLS/ Zeta potential are depicted in Figure 2B. The mean hydrodynamic diameters are 36.7 nm and 94.07 nm, and the polydispersity index (PDI) is 0.2 and 0.33 for Cs NPs and RSV. Cs NPs. Low PDI values demonstrated the homogenous distribution of NP suspensions. PDI value for RSV. Cs NPs was higher due to a minimal agglomeration observed during the measurement. Zeta potential values were 18.3 and 29.7 for Cs NPs and RSV. Cs NPs. RSV entrapment efficiency (EE) was $63 \pm 0.45\%$, reflecting more than 60% of initial RSV was entrapped in Cs NPs. The data for the RSV release is presented in Figure 2C. Upon the incubation of NPs in PBS at 37°C , an initial burst RSV release was observed in 3 hours when more than half of RSV ($57.62 \pm 3.5\%$) was released. Then, a sustained release was recorded up to 72 hours, reaching $93.7 \pm 2.9\%$.

Cell proliferation and IC₅₀ calculation

The MTT assay was performed to evaluate the inhibitory effects of RSV, Cs NPs, and RSV. Cs NPs on MDA-MB231 cell proliferation at 24, 48, and 72 hours (Fig.3). The data showed that all treatment groups inhibited cell proliferation in a concentration and time-dependent manner. Cs NPs and RSV. Cs NPs significantly reduced cell proliferation compared to the RSV group, among

which RSV. Cs NPs had the highest antiproliferative effect (**P<0.001). Following the MTT assay, dose-response curves were plotted for each treatment group, and IC₅₀ values were calculated. Dose-response curves and IC₅₀ graph are shown in Figure 4. IC₅₀ values at 24, 48, and 72 hours are 204.5, 122.4, and 64.82 µg/ml for RSV, 56.35, 23.65, and 13.9 for Cs NPs, and 33.75, 22.6, and 11.48 µg/ml for RSV. Cs NPs.

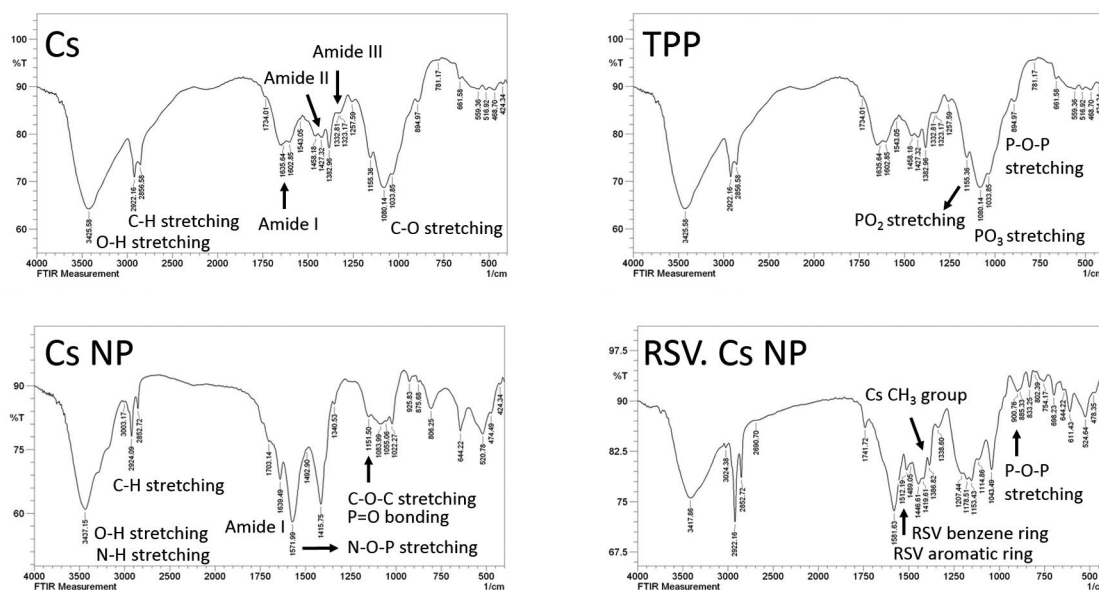


Fig.1: Chemical bonds related to Cs, TPP, RSV, and TPP Cross-linking were detected in synthesized NPs. FTIR; Fourier-transform infrared spectroscopy, Cs; Chitosan, TPP; Tripolyphosphate, RSV; Resveratrol, and NPs; Nanoparticles.

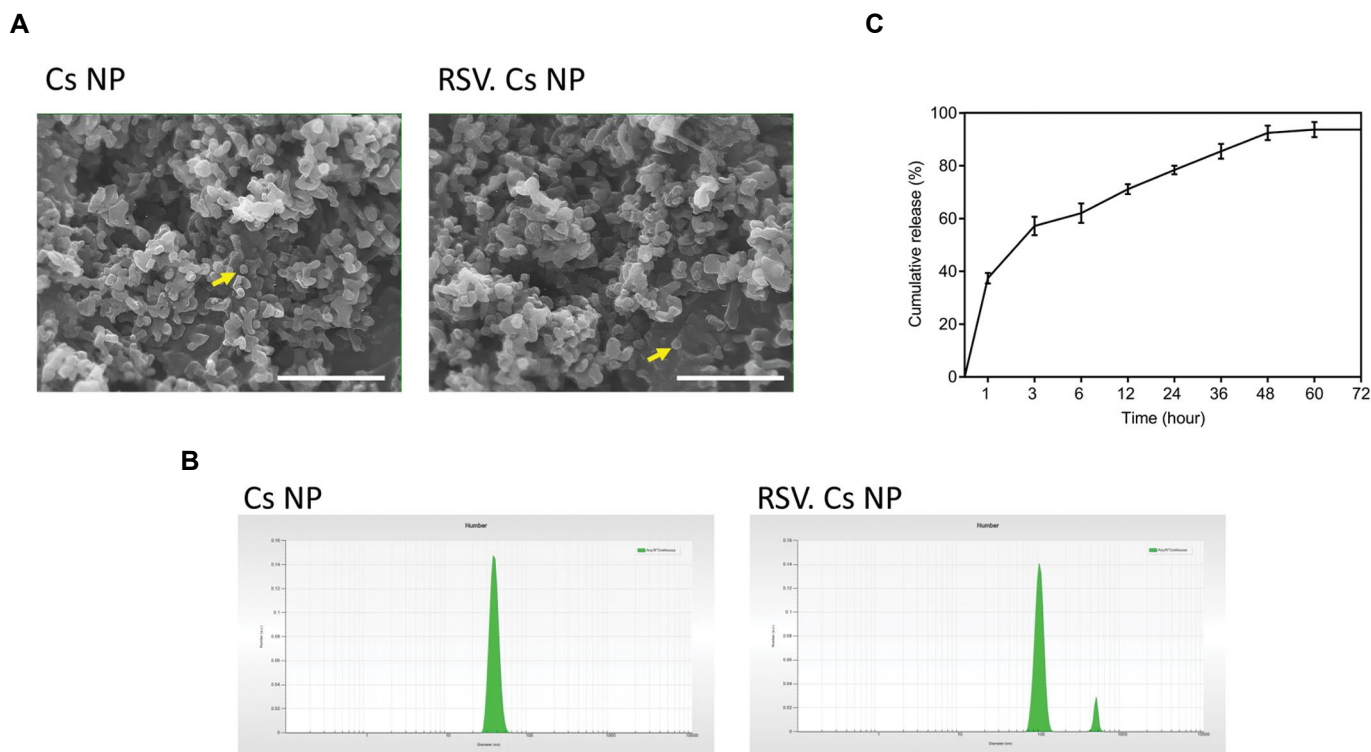


Fig.2: Morphological evaluations and size distribution analysis of Cs and RSV. Cs NPs. **A.** SEM micrographs of NPs with spherical shapes and smooth surfaces (yellow arrows, scale bar: 1 µm, 40000x). **B.** DLS data. **C.** In vitro RSV release. Cs; Chitosan, RSV; Resveratrol, NPs; Nanoparticles, SEM; Scanning electron microscope, and DLS; Dynamic light scattering.

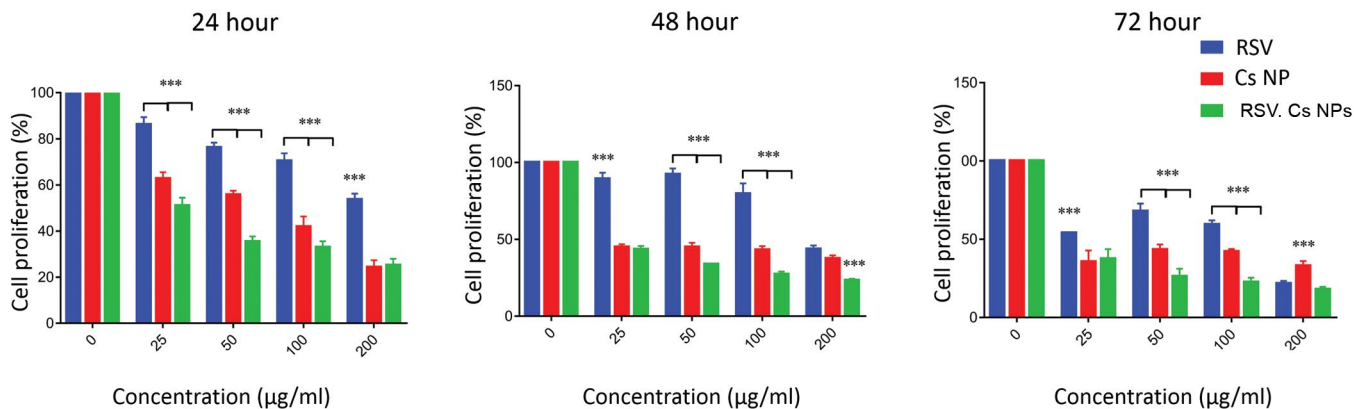


Fig.3: MTT data of MDA-MB231 cells treated with RSV, Cs NPs, and RSV. Cs NPs for 24, 48, and 72 hours. ***, P<0.001, MTT; 3-(4,5-Dimethylthiazol-2-yl)-2,5-diphenyltetrazolium bromide, RSV; Resveratrol, Cs; Chitosan, and NPs; Nanoparticles.

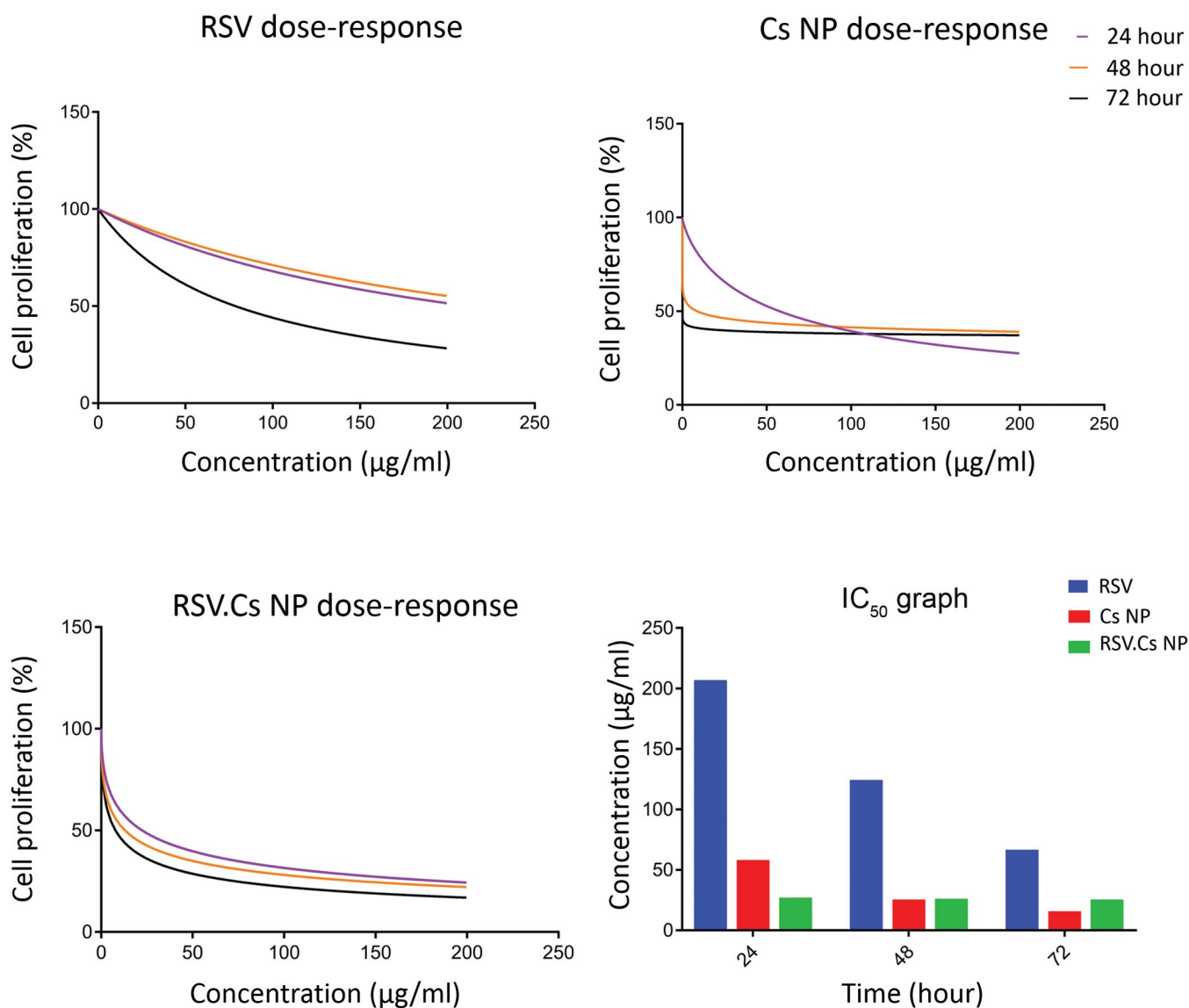


Fig.4: Dose-response curves and IC₅₀ values of RSV, Cs NPs, and RSV. Cs NPs at 24, 48, and 72 hours. IC₅₀; Half-maximal inhibitory concentration, RSV; Resveratrol, Cs; Chitosan, and NPs; Nanoparticles.

Cell viability

The cytotoxic effect of treatments against MDA-MB231 cells was evaluated by the LDH assay and reported as cell viability percentage (Fig.5). The

results showed that cell viability was reduced in all treatment groups due to concentration and time. Cs NPs and RSV. Cs NPs had higher toxicity than RSV, but significant differences were observed between RSV and RSV. Cs NPs (** $P < 0.001$, **** $P < 0.010$).

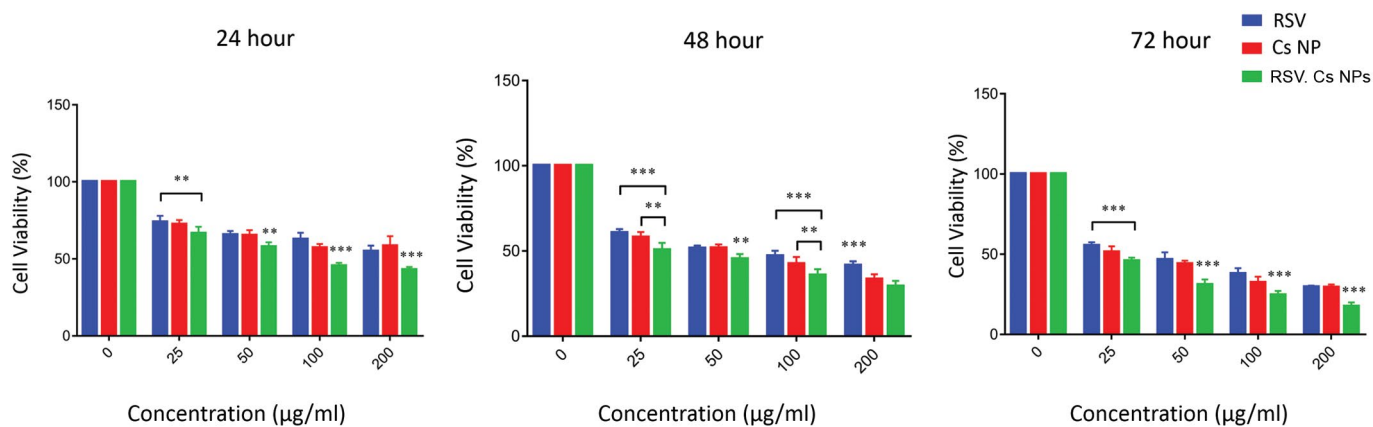


Fig.5: LDH assay and cell viability measurements of MDA-MB231 cells treated with RSV, Cs NPs, and RSV. Cs NPs for 24, 48, and 72 hours. ***, $P < 0.001$, **, $P < 0.01$, LDH; Lactate dehydrogenase, RSV; Resveratrol, Cs; Chitosan, and NPs; Nanoparticles.

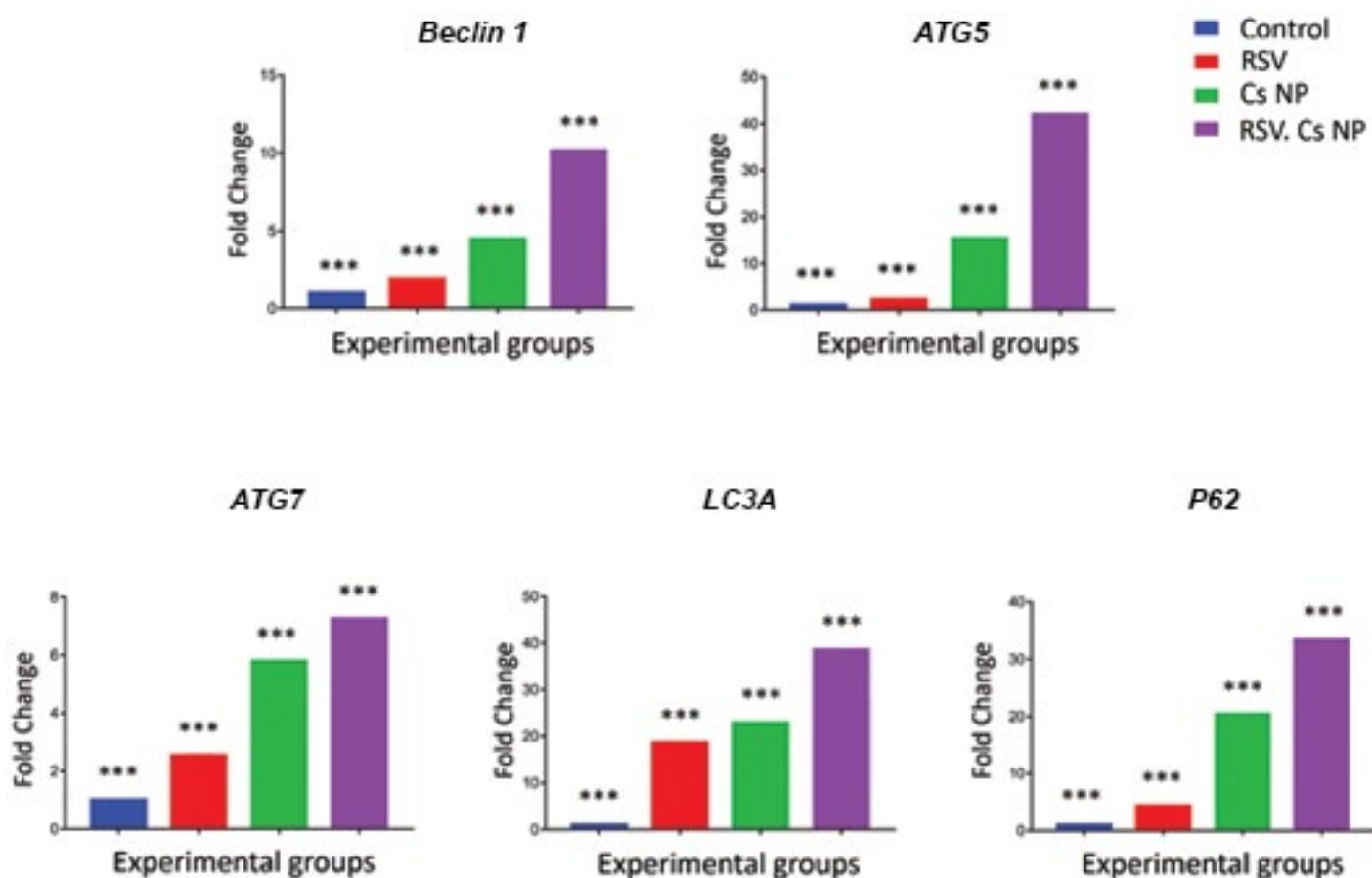


Fig.6: The assessment of autophagy induction in MDA-MB231 cells treated with IC_{50} concentrations of RSV, Cs NPs, and RSV. Cs NPs for 48 hours using real-time PCR. ***, $P < 0.001$, IC_{50} ; Half-maximal inhibitory concentration, RSV; Resveratrol, Cs; Chitosan, NPs; Nanoparticles, and PCR; Polymerase chain reaction.

Autophagy measurement

The expression of *Beclin-1*, *ATG-5*, *ATG-7*, *LC3A*, and *P62* autophagic genes was assessed in MDA-MB231 cells treated with IC_{50} concentrations of RSV, Cs NPs, and RSV. Cs NPs for 48 hours using the real-time PCR (Fig.6). The melting curves of genes of interest are shown in Figure S1 (See Supplementary Online Information at www.celljournal.org). Beclin-1 expression was higher in treatment groups than in control (untreated) cells. Beclin-1 expression was much higher in Cs NPs (4.47 folds) and RSV. Cs NPs (10.15 folds) than RSV (1.93 folds), and remarkable differences were observed among treatment groups ($***P<0.001$). ATG5 expression was significantly enhanced in treatment groups than in control (untreated) cells. ATG5 expression was boosted in cells incubated with Cs NPs (15.345 folds) and RSV. Cs NPs (41.93 folds) than RSV (2.25 folds), and all groups remarkably differed from each other ($***P<0.001$). ATG7 was expressed at higher levels in the treatment groups than in the control group. ATG7 levels increased in cells treated with Cs NPs (5.8 folds) and RSV. Cs NPs (7.25 folds) than RSV (2.53 folds), and notable differences were observed between groups ($***P<0.001$). LC3A overexpressed in treatment groups, and the highest expressions were observed in RSV. Cs NPs (38.55 folds), Cs NPs (22.9), and RSV (18.6), respectively. LC3A levels significantly differed between treatment groups ($***P<0.001$). P62 expression increased in treated cells in comparison with untreated cells. P62 values upgraded 33.4 folds in RSV. Cs NPs, 20.35 folds in Cs NPs, and 4.33 in RSV, where P62 expression remarkably differed between groups ($***P<0.001$). The results showed that Cs NPs and RSV. Cs NPs were more potent in inducing autophagy in MDA-MB cells than RSV.

Discussion

In the present study, we synthesized Cs NPs carrying RSV, a plant-derived polyphenol, using a simple ionic gelation method, characterized their physicochemical and biological properties, and evaluated their potential to inhibit MDA-MB231 BC cells by regulating autophagy. MDA-MB231 cells are a highly aggressive cell line established from a 51-year-old pleural effusion with a wide application in various aspects of BC research, like metastasis and drug resistance (22).

In our recent work, we showed that RSV. Cs NPs effectively suppressed MDA-MB231 cell growth by activating the intrinsic apoptotic pathway (19). However, the role of RSV in inducing cytoprotective or cytotoxic autophagy remains controversial, requiring more investigation. We used Cs NPs as appropriate carriers for the delivery, preserving the structural stability of RSV while providing a sustained release for up to 72 hours. Our findings showed that loading RSV into Cs NPs resulted in a synergistic anticancer effect with increased proliferation inhibition and autophagy stimulation. Although the interplay between Cs NPs and their cargos has not yet been

elucidated, Cs nanostructures could inhibit tumorigenesis by enhancing the drug/gene-targeted delivery and aggregation in tumor cells (23).

From FTIR data, peaks at 1207 cm^{-1} were detected belonging to cross-links between cationic amino groups of Cs and anionic phosphate groups of TPP, indicating Cs NPs were formed (24). Peaks at 3400 cm^{-1} are attributed to the stretching of hydroxyl groups and intramolecular hydrogen bonds. RSV incorporation resulted in much stretching reflecting hydrophobic interactions of RSV with NP components, and more hydrogen bonds were formed (25). Particle size is crucial in determining NP biocompatibility, bioactivity, anticancer effects, and intratumoral accumulation potential. Our results showed that NPs were morphologically sphere-shaped with smooth surfaces, and their size was less than 100 nm, appropriate for drug delivery and cellular penetration. NPs greater than 300 nm are unsuitable as they would be detected by the immune system and cleared from the blood circulation (26).

Zeta potential is a simple way to characterize the surface charge of nanosuspension colloids that could influence the structural stability and pharmacokinetic properties of NPs and their interactions with biological systems and cellular uptake (26). NPs had positive zeta potentials because of positively charged amino groups in the Cs matrix. Cs NPs could electrostatically interact with negatively charged phospholipid bilayer membranes and penetrate cells (16).

RSV entrapment efficiency was more than 60%, higher than our previous report, possibly due to the increased initial RSV concentration. This finding is consistent with an earlier study indicating that increasing initial concentrations led to higher amounts of ferulic acid entrapping within Cs NPs (25). The assessment of RSV release showed that more than half of RSV released from NPs within 3 hours, followed by a gradual release up to 72 hours. The burst release might be a function of RSV molecules' desorption, diffusion, and dissolution on the surface of NPs. In contrast, gradual release depends on the excretion of RSV molecules within the NP matrix (27).

MTT data showed that Cs NPs were more efficient in inhibiting cell growth than the equivalent quantities of RSV. Also, IC_{50} values significantly reduced in pure and RSV. Cs NPs compared to RSV, suggesting that nanoformulations augmented the antiproliferative effects of RSV by improving physicochemical and biological properties, including bioavailability and dissolution, and providing controlled release (28). Cs NP had a more substantial impact in suppressing cell proliferation even at low concentrations, which was attributed to higher reactive oxygen species (ROS) production (29).

Autophagy is a highly conserved metabolic pathway in eukaryotic cells associated with degrading damaged organelles and cytoplasmic components like lipids,

proteins, and inclusion bodies and recycling them into whole organelles (30). The role of autophagy in progressing or inhibiting BC remains controversial; on the one hand, autophagy protects cells from death by removing damaged cellular components and regulating the cell cycle. On the other hand, autophagy hyperactivity and broad depletion of cytoplasmic constituents give rise to apoptosis and necrosis. However, evidence suggests that autophagy might act as a tumor suppressor in fully transformed cells, and defective autophagy is linked to malignant transformation and carcinogenesis (31).

The gene expression evaluations showed that treatment with either RSV or NPs could increase the autophagy-related expression of *Beclin-1*, *ATG-5*, *ATG-7*, *LC3A*, and *P62*. NPs had a more potent effect in inducing autophagy in which RSV. Cs NPs had the most significant impact. A previous study showed RSV could induce autophagy in 4T1 BC cells by upregulating the SIRT3/MAPK signaling pathway (32). *Beclin-1* is a haploinsufficient tumor suppressor participating in initial phagophore complexes and is deleted in 40-75% of sporadic breast and ovarian cancer cases in a monoallelic manner (33). Treatments enhanced *Beclin-1* expression, consistent with a previous study that showed RSV could induce *Beclin-1* and LC3B in A459 lung cancer cells by upregulating the NGFR-AMPK pathway and inhibiting the mTOR pathway (34).

ATG-5 is a critical protein in extending phagophoric membranes activated by ATG-7 and could also act as a pro-apoptotic molecule. ATG-5 inhibition is linked to increased BC cell proliferation, migration, and invasion (35). In our study, high ATG-5 and ATG-7 expression was observed in cells treated with NPs, demonstrating the nanocarriers' potential to enhance the therapeutic effects of RSV. RSV-mediated ATG-5 expression resulted in the activation of caspase cascades and apoptosis induction in ovarian cancer cells (36).

LC3A is a key protein involved in autophagosome formation and elongation that converts into LC3B as a function of ATG-5/ATG-7 complex activity. Our results revealed that LC3A overexpressed in cells treated with RSV, Cs NPs, and RSV. Cs NPs. We believe that abnormal overexpression of LC3A reflects that intracellular components are degrading at high rates, which impairs the balance between degradation and recycling rates. Finally, unlimited destruction of cytoplasmic components drives cell death and apoptosis.

P62 is a scaffolding protein responsible for transferring ubiquitinated proteins into autophagosomes. In our experiment, P62 expression increased markedly, which could lead to accumulating P62/ubiquitinated protein complexes within autophagosomes. Some phytochemicals have been found to prevent P62 degradation by reducing the expression of lysosomal proteases and cathepsins. P62 aggregation is associated with ROS production and apoptosis-mediated cell death (37). RSV was demonstrated to induce P62 accumulation-mediated ROS

generation and apoptosis in chronic myeloid leukemia cells by upregulating the JNK signaling pathway (38).

Conclusion

Cs NPs are efficient delivery systems for increasing RSV bio-availability and augmenting its anticancer effects by stimulating autophagy in BC cells *in vitro*, which could be considered novel future therapeutic strategies. Also, novel multi-drug delivery systems and combination strategies of NPs with conventional therapeutics are suggested to be explored. However, more *in vitro* and *in vivo* pre-clinical studies are highly recommended to uncover all aspects of the safety, efficacy, and long-term outcomes of administered NPs.

Acknowledgements

The authors acknowledge the Fertility and Infertility Research Center, Health Technology Institute, Kermanshah University of Medical Sciences, Kermanshah, Iran, for their equipment and facilities support. This work was financially supported by the Kermanshah University of Medical Sciences, Kermanshah, Iran (grant No. 4020021). The authors declare that there is no conflict of interest.

Authors' Contributions

A.B.; Conceptualization, Investigation, Formal analysis, Writing-Original draft preparation, and Funding acquisition. M.R.Kh.; Supervision, Data Curation, Formal analysis, Writing-Review and Editing. M.B., M.Kh., M.A.; Methodology, Investigation, Formal analysis, Writing-Review and Editing. All authors read and approved the final manuscript.

References

1. Sung H, Ferlay J, Siegel RL, Laversanne M, Soerjomataram I, Jemal A, et al. Global cancer statistics 2020: GLOBOCAN estimates of incidence and mortality worldwide for 36 cancers in 185 countries. *CA Cancer J Clin*. 2021; 71(3): 209-249.
2. Anderson BO, Ilbawi AM, Fidarova E, Weiderpass E, Stevens L, Abdel-Wahab M, et al. The global breast cancer initiative: a strategic collaboration to strengthen health care for non-communicable diseases. *Lancet Oncol*. 2021; 22(5): 578-581.
3. Arnold M, Morgan E, Rumgay H, Mafra A, Singh D, Laversanne M, et al. Current and future burden of breast cancer: global statistics for 2020 and 2040. *Breast*. 2022; 66: 15-23.
4. Mirza Z, Karim S. Nanoparticles-based drug delivery and gene therapy for breast cancer: Recent advancements and future challenges. *Semin Cancer Biol*. 2021; 69: 226-237.
5. Younas M, Hano C, Giglioli-Guivarc'h N, Abbasi BH. Mechanistic evaluation of phytochemicals in breast cancer remedy: current understanding and future perspectives. *RSC Adv*. 2018; 8(52): 29714-29744.
6. Gil-Martínez L, Mut-Salud N, Ruiz-García JA, Falcón-Piñeiro A, Maijón-Ferré M, Baños A, et al. Phytochemicals determination, and antioxidant, antimicrobial, anti-inflammatory and anticancer activities of blackberry fruits. *Foods*. 2023; 12(7): 1505.
7. Noori F, Osanloo M, Moradi HR, Ghaderi Jafarbeigloo H, Jireh-nezhadyan M, Kouhpayeh SA, et al. Fabrication, characterization, and *in vivo* implantation of eugenol-loaded nanogels and PCL/Cs electrospun nanofibers for wound healing applications. *J Bioact Compat Polym*. 2023; 38(6): 480-492.
8. Shrikanta A, Kumar A, Govindaswamy V. Resveratrol content and antioxidant properties of underutilized fruits. *J Food Sci Technol*. 2015; 52(1): 383-390.
9. Abdal Dayem A, Choi HY, Yang GM, Kim K, Saha SK, Cho SG. The

- anti-cancer effect of polyphenols against breast cancer and cancer stem cells: molecular mechanisms. *Nutrients*. 2016; 8(9): 581.
10. Huang X, Dai Y, Cai J, Zhong N, Xiao H, McClements DJ, et al. Resveratrol encapsulation in core-shell biopolymer nanoparticles: Impact on antioxidant and anticancer activities. *Food Hydrocoll*. 2017; 64: 157-165.
 11. Chuan L, Zhang J, Yu-Jiao Z, Shu-Fang N, Jun C, Qian W, et al. Biocompatible and biodegradable nanoparticles for enhancement of anti-cancer activities of phytochemicals. *Chinese J Nat Med*. 2015; 13(9): 641-652.
 12. Osanloo M, Noori F, Tavassoli A, Ataollahi MR, Davoodi A, Seifalah-Zade M, et al. Effect of PCL nanofiber mats coated with chitosan microcapsules containing cinnamon essential oil for wound healing. *BMC Complement Med Ther*. 2023; 23(1): 84.
 13. Jain V, Kumar H, Anod HV, Chand P, Gupta NV, Dey S, et al. A review of nanotechnology-based approaches for breast cancer and triple-negative breast cancer. *J Control Release*. 2020; 326: 628-647.
 14. Katiyar SS, Muntimadugu E, Rafeeqi TA, Domb AJ, Khan W. Co-delivery of rapamycin-and piperine-loaded polymeric nanoparticles for breast cancer treatment. *Drug Deliv*. 2016; 23(7): 2608-2616.
 15. Khan MA, Zafaryab M, Mehdi SH, Quadri J, Rizvi MM. Characterization and carboplatin loaded chitosan nanoparticles for the chemotherapy against breast cancer in vitro studies. *Int J Biol Macromol*. 2017; 97: 115-122.
 16. Mirzaie ZH, Irani S, Mirfakhraie R, Atyabi SM, Dinarvand M, Dinarvand R, et al. Docetaxel-chitosan nanoparticles for breast cancer treatment: cell viability and gene expression study. *Chem Biol Drug Des*. 2016; 88(6): 850-858.
 17. Sachdeva B, Sachdeva P, Negi A, Ghosh S, Han S, Dewanjee S, et al. Chitosan nanoparticles-based cancer drug delivery: application and challenges. *Mar Drugs*. 2023; 21(4): 211.
 18. de Oliveira Pedro R, Hoffmann S, Pereira S, Goycoolea FM, Schmitt CC, Neumann MG. Self-assembled amphiphilic chitosan nanoparticles for quercetin delivery to breast cancer cells. *Eur J Pharm Biopharm*. 2018; 131: 203-210.
 19. Bozorgi A, Haghghi Z, Khazaei MR, Bozorgi M, Khazaei M. The anti-cancer effect of chitosan/resveratrol polymeric nanocomplex against triple-negative breast cancer; an in vitro assessment. *IET Nanobiotechnol*. 2023; 17(2): 91-102.
 20. Wu J, Wang Y, Yang H, Liu X, Lu Z. Preparation and biological activity studies of resveratrol loaded ionically cross-linked chitosan-TPP nanoparticles. *Carbohydr Polym*. 2017; 175: 170-177.
 21. Taghi GM, Ghasem Kashani Maryam H, Taghi L, Leili H, Leyla M. Characterization of in vitro cultured bone marrow and adipose tissue-derived mesenchymal stem cells and their ability to express neurotrophic factors. *Cell Biol Int*. 2012; 36(12): 1239-1249.
 22. Huang Z, Yu P, Tang J. Characterization of triple-negative breast cancer MDA-MB-231 cell spheroid model. *Onco Targets Ther*. 2020; 13: 5395-5405.
 23. Ferreira Tomaz A, Sobral de Carvalho SM, Cardoso Barbosa R, L. Silva SM, Sabino Gutierrez MA, B. de Lima AG, et al. Ionically crosslinked chitosan membranes used as drug carriers for cancer therapy application. *Materials (Basel)*. 2018; 11(10): 2051.
 24. Panwar R, Sharma AK, Kaloti M, Dutt D, Pruthi V. Characterization and anticancer potential of ferulic acid-loaded chitosan nanoparticles against ME-180 human cervical cancer cell lines. *Appl Nanosci*. 2016; 6(6): 803-813.
 25. Herdiana Y, Wathoni N, Shamsuddin S, Joni IM, Muchtaridi M. Chitosan-based nanoparticles of targeted drug delivery system in breast cancer treatment. *Polymers*. 2021; 13(11): 1717.
 26. Senthil Kumar C, Thangam R, Mary SA, Kannan PR, Arun G, Madhan B. Targeted delivery and apoptosis induction of trans-resveratrol-ferulic acid loaded chitosan coated folic acid conjugate solid lipid nanoparticles in colon cancer cells. *Carbohydr Polym*. 2020; 231: 115682.
 27. Al-Jubori AA, Sulaiman GM, Tawfeeq AT, Mohammed HA, Khan RA, Mohammed SA. Layer-by-layer nanoparticles of tamoxifen and resveratrol for dual drug delivery system and potential triple-negative breast cancer treatment. *Pharmaceutics*. 2021; 13(7): 1098.
 28. Khatun M, Choudhury S, Liu B, Lemmens P, Pal SK, Mazumder S. Resveratrol-ZnO nanohybrid enhanced anti-cancerous effect in ovarian cancer cells through ROS. *RSC Adv*. 2016; 6(107): 105607-105617.
 29. Li T, Ashrafizadeh M, Shang Y, Nuri Ertas Y, Orive G. Chitosan-functionalized bioplatfroms and hydrogels in breast cancer: immunotherapy, phototherapy and clinical perspectives. *Drug Discov Today*. 2024; 29(1): 103851.
 30. Cassidy LD, Young ARJ, Young CNJ, Soilleux EJ, Fielder E, Weigand BM, et al. Temporal inhibition of autophagy reveals segmental reversal of ageing with increased cancer risk. *Nat Commun*. 2020; 11(1): 307.
 31. Zarzynska JM. The importance of autophagy regulation in breast cancer development and treatment. *Biomed Res Int*. 2014; 2014: 710345.
 32. Wang J, Huang P, Pan X, Xia C, Zhang H, Zhao H, et al. Resveratrol reverses TGF- β 1-mediated invasion and metastasis of breast cancer cells via the SIRT3/AMPK/autophagy signal axis. *Phytother Res*. 2023; 37(1): 211-230.
 33. Singh S, Nguyen H, Michels D, Bazinet H, Matkar PN, Liu Z, et al. BReast CAncer susceptibility gene 2 deficiency exacerbates oxidized LDL-induced DNA damage and endothelial apoptosis. *Physiol Rep*. 2020; 8(13): e14481.
 34. Li J, Fan Y, Zhang Y, Liu Y, Yu Y, Ma M. Resveratrol induces autophagy and apoptosis in non-small-cell lung cancer cells by activating the NGFR-AMPK-mTOR pathway. *Nutrients*. 2022; 14(12): 2413.
 35. Liang Y, Pi H, Liao L, Tan M, Deng P, Yue Y, et al. Cadmium promotes breast cancer cell proliferation, migration and invasion by inhibiting ACSS2/ATG5-mediated autophagy. *Environ Pollut*. 2021; 273: 116504.
 36. Lang F, Qin Z, Li F, Zhang H, Fang Z, Hao E. Apoptotic cell death induced by resveratrol is partially mediated by the autophagy pathway in human ovarian cancer cells. *PLoS One*. 2015; 10(6): e0129196.
 37. Choi YK, Cho SG, Choi YJ, Yun YJ, Lee KM, Lee K, et al. SH003 suppresses breast cancer growth by accumulating p62 in autolysosomes. *Oncotarget*. 2017; 8(51): 88386-88400.
 38. Jang JY, Im E, Kim ND. Mechanism of resveratrol-induced programmed cell death and new drug discovery against cancer: a review. *Int J Mol Sci*. 2022; 23(22): 13689.